A New Multiferroic State with Large Electric Polarization in Tensile Strained

TbMnO₃

Y. S. Hou, J. H. Yang, X. G. Gong^{*}, and H. J. Xiang^{*}

¹ Key Laboratory of Computational Physical Sciences (Ministry of Education), State

Key Laboratory of Surface Physics, and Department of Physics, Fudan University,

Shanghai 200433, P. R. China

Abstract

By performing first-principles calculations, we systematically explore the effect of

epitaxial strain on the structure and properties of multiferroic TbMnO₃. We show that,

although the unstrained bulk TbMnO₃ displays a non-collinear antiferromagnetic spin

order, TbMnO₃ can be ferromagnetic under compressive strain, in agreement with the

experimental results on TbMnO₃ grown on SrTiO₃. By increasing the tensile strain up

to 5%, we predict that TbMnO₃ transforms into a new multiferroic state with a large

ferroelectric polarization, two orders of magnitude larger than that in the unstrained

bulk, and with a relatively high Neel temperature E-type antiferromagnetic order. We

also find that the ferroelectric domain and antiferromagnetic domain are interlocked

with each other, thus an external electric field can switch the ferroelectric domain and

the antiferromagnetic domain simultaneously. Our work demonstrates that strain

engineering can be used to improve the multiferroic properties of TbMnO₃.

Multiferroic materials [1-2], displaying two or more orders of magnetic, polar, and elastic order simultaneously, have attracted much attention due to their potential applications as novel devices [3]. In these materials, the spin order and electric polarization can be controlled by the external electric field and magnetic field, respectively [4]. TbMnO₃, as a typical orthorhombic perovskite multiferroic material, has been the research topic of many studies, since Kimura *et al.* discovered the switch of ferroelectric polarization by magnetic fields [5]. The spins of Mn³⁺ ions in bulk *Pbnm* TbMnO₃ form an incommensurate cycloidal spin spiral below $T_{lock} \approx 28~K$ [6], and a polarization of $\sim 0.06~\mu\text{C}/cm^2$ simultaneously appears along *c*-direction [7]. The polarization was found to be a consequence of spin-orbit coupling [8-9] and dominated by the contributions from the ion displacements [10-12]. Although there is a strong intrinsic magnetoelectric coupling in bulk TbMnO₃, the transition temperature is too low and the electric polarization is too small for realistic applications.

Recently, it has been demonstrated experimentally that unexpected anomalous ferromagnetism appears in (001)-oriented TbMnO₃ thin film epitaxially grown on the (001) plane of the cubic substrate SrTiO₃ (STO) [13]. Besides, RMnO₃ (R represents a rare-earth element) displays various spin orders with decreasing ion radius of R, i.e., LaMnO₃, TbMnO₃, and HoMnO₃ display the A-type antiferromagnetic (AFM) order, the non-collinear spiral order, and the E-type AFM order, respectively [14-15]. In addition, it was found that epitaxial strain could be used to tune the magnetic and

polar order of perovskite magnetic oxides such as EuTiO₃ [16-17].

In this Letter, we propose to use epitaxial strain to tune the multiferroic properties of TbMnO₃. Our density functional calculations show that when TbMnO₃ is grown on SrTiO₃, the ground state is ferromagnetic (FM) with the centrosymmetric orthorhombic *Pbnm* space group, in agreement with experiments [13]. When the epitaxial tensile strain reaches 5%, the ground state of TbMnO₃ transforms into a new multiferroic state, i.e., insulating E-type AFM state with polar orthorhombic $Pmc2_1$ space group. This new $Pmc2_1$ -E-AFM state is characterized by a large electric polarization of 4.56 μ C/cm² and a relatively high Neel transition temperature above 100 K. The E-AFM spin order is interlocked with the polar order, thus we propose a feasible strategy to switch the AFM domains through an applied electric field.

Our study is based on first-principles density functional theory (DFT) calculations [18]. We assume that TbMnO₃ is grown on the (001)-oriented cubic substrates. Hence epitaxial strain is defined as $\eta = \frac{a-a_0}{a_0}$ where a and a_0 are the in-plane lattice constants of the epitaxially strained and free-standing TbMnO₃ in cubic state [19]. As usual, we consider several common magnetic orders in perovskite, namely FM, A-type AFM (A-AFM), C-type AFM (C-AFM), G-type AFM (G-AFM), and E-type AFM (E-AFM) spin orderings. We double the unit cell in a- or b-direction to allow E-AFM magnetic order. For each strain and each magnetic order, structural relaxation begins with the initial structure with Pbnm space group and the in-plane lattice constants are fixed while the out-of-plane lattice constant and internal ionic coordinates are fully relaxed without imposing any symmetry. This strategy was

shown to be successful in finding the ground state of the epitaxially strained perovskite oxides such as $SrRuO_3$ and $BiFeO_3$ [20]. For the E-AFM order, the unit cell is energetically preferred to be doubled along the *b*-axis in the case of compressive and small tensile strain, while the unit cell is preferred to be doubled along the *a*-axis in the case of tensile strain larger than 1%.

According to the definition, TbMnO₃ experiences 1% compressive strain when grown on the cubic substrate STO. Our calculations show that its ground state is ferromagnetic (see Fig. 1), in agreement with experiments [13]. This FM ground state is also consistent with the symmetric exchange interactions between spins of Mn³⁺ ions, which are defined in Ref. 11. Our calculated results [21] show that the in-plane nearest neighboring interaction J_{ab} is strongly FM and its magnitude is much larger than that of the in-plane next nearest neighboring interaction J_{aa} and J_{bb}, indicating that the spins of Mn³⁺ ions align ferromagnetically in the (001) planes. Interestingly, the magnetic interaction along *c*-direction is also FM, different from the bulk case.

The appearance of ferromagnetism in epitaxially strained TbMnO₃ is due to the change of the electronic structure as discussed below. In bulk RMnO₃, each Mn³⁺ ion has four unpaired d electrons: three of them occupy the low-energy t_{2g} orbitals and the remaining one occupies the high-energy e_g orbitals. Because of the Jahn-Teller distortion, the two degenerate e_g states on each spin site split into two non-degenerate orbitals and only one is occupied. The occupied e_g orbitals on two adjacent spin sites are almost orthogonal to each other in the ab-plane. However, the orbital order in epitaxially strained TbMnO₃ is revealed to be dramatically different:

the two e_g orbitals on each spin site are almost degenerate and can be seen as both half occupied (see Fig. 2), i.e., the electron configuration of each $\mathrm{Mn}^{3+}(d^4)$ ion can be roughly described as $(t_{2g})^3(d_{3z^2-r^2})^{\frac{1}{2}}(d_{x^2-y^2})^{\frac{1}{2}}$. This electron configuration is consistent with the shape of the MnO₆ octahedron (see the insert in Fig. 2): All the Mn-O bond lengths are of similar magnitude and the O-Mn-O bond angles are close to 90^o or 180^o . Now, let us examine the interaction between the e_g orbitals of two adjacent spin sites (1 and 2) along c-direction for the cases of both FM and AFM arrangements. In the FM case (see Fig. 2), the majority-spin e_g (d_{z^2}) orbitals of site 1 and 2 with the same energy level can couple with each other, forming an empty higher energy level and an occupied lower energy level, thereby lowering the total energy by t, where t > 0 is the hopping integral between these two d_{z^2} orbitals. In the AFM case (see Fig. 2), the majority-spin e_g orbital of one Mn site couples the minority-spin e_g orbital of the other Mn site. In this case, the total energy lowering is $\frac{U}{2} - \sqrt{t^2 + \frac{U^2}{4}}$, where U (>0) is the energy difference between e_g orbitals with opposite spin components. It is clear that the FM state has a lower energy. The same mechanism also applies to the in-plane exchange interaction Jab. Thus, the epitaxially strained TbMnO₃ prefers to interact ferromagnetically. In addition, the nearest neighboring Mn-Mn distances decrease and the Mn-O-Mn angles become larger with respect to those of bulk, which enhance the coupling of e_g orbitals (increase of t) and thereby increase the magnitude of spin exchange interaction parameters. This is consistent with the increasing of the symmetric spin exchange parameters [21].

We now discuss the ground states as the epitaxial strain varies. The dependence of

the total energy of one formula unit (f.u.) upon the epitaxial strain is shown in Fig. 1. Our calculated results show that the C-AFM and G-AFM spin orders almost always have higher energy than others (not shown in Fig. 1. for simplicity). In the compressive epitaxial strain region, TbMnO₃ is metallic FM, distinctly different from the insulating AFM bulk. At the 0% strain, there is a first-order isosymmetric phase transition [22] between two *Pbnm*-FM states, which is also confirmed by analyzing the Jahn-Teller distortion (see Part 2 of [18]). A gap opens when the tensile strain is higher than 1% (see the inset of Fig. 1).

Interestingly, when the tensile strain is larger than $\approx 4.5\%$, the ground state is E-type ordering with a polar Pmc2₁ space group. In this E-AFM order, the FM zigzag chain is along the b-axis (Fig. 3a), which is different from that along the a-axis in the Pbnm-E-AFM HoMnO₃ case [23]. The evolution of the geometrical structure with E-AFM spin order is shown in Figs. 3(d) and 3(e). Before the E-AFM spin order is adopted as the ground state, there is only a small difference between the in-plane Mn-Mn bond distance along zigzag chains and that between two neighboring zigzag chains. However, when TbMnO₃ adopts the E-AFM spin order as the ground state, the difference is as large as 0.8 Å. Moreover, the Mn-O-Mn bond angles α_p [see Figs. 3(a)] along zigzag chains are closer to 180^{o} than the Mn-O-Mn bond angles α_{ap} [see Fig. (3a)] between two neighboring zigzag chains, which is similar to the case of Pbnm-E-AFM HoMnO₃ [23]. This is due to the fact that the 180° Mn-O-Mn bond leads to an increased hopping between the occupied e_g orbital and the unoccupied e_g orbital. It is worth noting that an O-Mn-O bond angle severely deviates from 180° in the MnO₆ octahedron of $Pmc2_I$ -E-AFM TbMnO₃, different from the case of Pbnm-E-AFM HoMO₃ [see Figs. 3(b) and 3(c)]. These indicate that epitaxially strained $Pmc2_I$ TbMnO₃ displays substantial lattice distortions.

In order to understand why this new Pmc2₁-E-AFM state becomes the ground state, we decompose the total energy E_{tot} into the elastic energy E_e (including Coulomb electrostatic interaction, i.e., Madelung energy), and the magnetic energy E_m originating from spin exchange interactions, namely $E_{tot} = E_e + E_m$. In $Pmc2_I$ structure, four different in-plane exchange paths (see Fig. 3a) and two different paths along c-direction (not shown) are considered, i.e., J_{ab1} , J_{ab2} , J_{aa} , J_{bb} , J_{cc1} and J_{cc2} . By calculating spin exchange parameters and the total energy, we can obtain the elastic energy E_e and magnetic energy E_m . The calculated results in the case of 5% tensile strain are listed in Table I. While the magnetic energy E_m of Pbnm-FM state is lower than that of $Pmc2_1$ -E-AFM state, the elastic energy E_e of Pbnm-FM state is much higher than that of Pmc2₁-E-AFM state. This indicates that the Pmc2₁ structure is much softer than the Pbnm structure, which is consistent with the results on tensile strained BiFeO₃ [20] and with that *Pbnm* structure has a higher Madelung energy than Pmc2₁ structure (see Part 4 of [18]). In addition, Pmc2₁-FM state has a higher magnetic energy E_m than that of $Pmc2_1$ -E-AFM state, which indicates that in the Pmc2₁ structure the E-AFM spin order is preferred over the FM spin order. Hence, this new Pmc2₁-E-AFM state found in the tensile strained TbMnO₃ is a cooperative result of the softness of the Pmc2₁ structure and compatible spin exchange interactions.

This new Pmc2₁-E-AFM state is insulating and polar, thus it could be ferroelectric. Using the E-AFM spin order [23], our Berry phase calculation shows that the electric polarization is as large as $4.56 \mu C/cm^2$ along the zigzag chain, i.e., the positive b-axis. The large electric polarization in Pmc2₁-E-AFM state is almost two orders of magnitude larger than that in bulk TbMnO₃. It was well-known that the total electric polarization (P_{tot}) in multiferroics contains both the electronic contribution (P_{ele}) and the ionic contribution (P_i) , i.e. $P_{tot} = P_{ele} + P_i$. To separate these two contributions, we directly calculate the electronic contribution P_{ele} due to the E-AFM spin order in this new Pmc2₁-E-AFM state using the model proposed in Ref. 2 and get that the electronic contribution P_{ele} is $-0.64 \, \mu \text{C}/\text{cm}^2$. Thus, the ionic contribution P_i due to ion displacements from centrosymmetric positions is $5.20~\mu\text{C}/cm^2$, dominating in the total electric polarization P_{tot} . Note that the non-negligible negative electronic contribution will result in a negative magnetoelectric effect [24]. This is dramatically different from the case of Pbnm-E-AFM HoMnO₃ where the electronic contribution is in the same direction and has a similar magnitude as the ionic contribution [23]. Detailed calculations (see Part 3 of [18]) reveal that the positive ionic contribution is dominated by Terbium ions' contributions. Further investigations evidence that such positive ionic contribution is favored by Coulomb electrostatic interaction (see Part 4 of [18]). As for the negative electronic contribution, it is due to the homogenous positive b-direction migration of e_q electrons from the occupied d_{z^2} orbital of one Mn^{3+} ion to the unoccupied $d_{x^2-y^2}$ orbital of its nearest neighboring $\,\mathrm{Mn}^{3+}\,$ ion in the FM zigzag chains (see Part 5 of [18]).

We now examine the magnetic transition temperature. The Neel temperature T_N of this new $Pmc2_I$ -E-AFM state can be approximated by solving E_H with mean field theory [25]: $T_N = \frac{2}{3}S(S+1)(J_1z_1-J_2z_2-J_3z_3-J_4z_4+J_5z_5-J_6z_6) \approx 247$ K. We also perform Monte Carlo (MC) simulations to find that the transition temperature T_N is about 100~K (see Part 6 of [18]). It is well-known that the mean field theory overestimates and the MC simulation underestimates the transition temperature, respectively. Thus, we expect that the Neel temperature is close to 150 K. Compared with bulk TbMnO₃ ($T_N \approx 28~K$), the transition temperature in this new $Pmc2_I$ -E-AFM state is much higher.

Finally, there are two different E-type spin orders (E1 and E2) [23, 26], i.e. two different AFM domains, in the tensile strained TbMnO₃. These two AFM domains have equal-magnitude but opposite electric polarizations. In addition, these two domains have one-to-one correspondence relationship with the directions of electric polarizations, denoted as +P(E1) and -P(E2) (see Part 7 of [18]). We investigated the switching between them. In HoMnO₃, a 180° coherent progressive rotation of spins of Mn³⁺ ions was proposed to switch these two domains [26]. However, this mechanism may be not suitable to the case of the epitaxially strained TbMnO₃ because the polarization is dominated by ion displacements but not by the E-AFM order. Hence, we propose another suitable mechanism in the structural space. We starts with +P(E1) lattice structure, then the ions' positions are slightly displaced step by step toward to -P(E2) lattice structure. This path must pass through a

centrosymmetric paraelectric phase. In each movement step, the magnetic order with the lowest energy for a giving geometrical structure is considered. Using this strategy, we find that the depth of the well is ≈ 75 meV/ f.u. (see Part 7 of [18]), which is smaller than the value ≈ 200 meV/f.u. in the case of PbTiO₃ [27]. In fact, the calculated energy barrier is an upper limit for experiments. Hence, we show that it's possible to use an external electric field to switch the two E-AFM domains experimentally.

In summary, our first-principles results show that, although unstrained bulk TbMnO₃ prefers to be insulating antiferromagnetic, compressed strained TbMnO₃ can be ferromagnetic, in agree with experiments [13]. The appearance of ferromagnetism is attributed to the change of electronic structure with respect to bulk TbMnO₃. Of the most importance is that, when TbMnO₃ experiences an epitaxial strain larger than $\approx 4.5\%$, a phase transition from paraelectric ferromagnetic order into ferroelectric E-type antiferromagnetic order takes place, resulting in a polarization as large as $4.56 \,\mu\text{C/cm}^2$ and a relatively high transition temperature above $100 \, K$. Furthermore, we found that in the tensile strained TbMnO₃, the E-type magnetic order is coupled with the polar order, thus it is possible to manipulate the two different antiferromagnetic domains through an external electric field. These show that one can engineer TbMnO₃ as fascinating perovskite multiferroic material by substrate-induced epitaxial strain.

Work at Fudan was partially supported by NSFC, the Special Funds for Major State Basic Research, Foundation for the Author of National Excellent Doctoral

Dissertation of China, The Program for Professor of Special Appointment at Shanghai Institutions of Higher Learning, Research Program of Shanghai municipality and MOE. We thank X. Z. Lu and Z. L. Li for useful discussions.

E-mail: xggong@fudan.edu.cn, hxiang@fudan.edu.cn

Reference

- [1] W. Eerenstein, N. D. Mathur and J. F. Scott, Nature (London) 442, 759 (2006).
- [2] H. J. Xiang, E. J. Kan, Y. Zhang, M.-H. Whangbo and X. G. Gong, Phys. Rev. Lett. 107, 157202 (2011); X. Z. Lu, M.-H. Whangbo, Shuai Dong, X. G. Gong and H. J. Xiang, Phys. Rev. Lett. 108, 187204 (2012).
- [3] Yoshinori Tokura, Science **312**, 1481 (2006).
- [4] N. Hur, S. Park, P. A. Sharma, J. S. Ahn, S. Guha and S-W. Cheong, Nature (London) **429**, 392 (2004).
- [5] T. Kimura, T. Goto, H. Shintani, K. Ishizaka, T. Arima and Y. Tokura, Nature (London) **426**, 55 (2003).
- [6] R. Kajimoto, H. Yoshizawa, H. Shintani, T. Kimura and Y. Tokura, Phys. Rev. B 70, 012401 (2004).
- [7] O. Prokhnenko, R. Feyerherm, E. Dudzik, S. Landsgesell, N. Aliouane, L. C. Chapon and D. N. Argyriou, Phys. Rev. Lett. **98**, 057206 (2007).
- [8] H. Katsura, N. Nagaosa and A. V. Balatsky, Phys. Rev. Lett. 95, 057205 (2005).
- [9] M. Mostovoy, Phys. Rev. Lett. 96, 067601 (2006).
- [10] I. A. Sergienko and E. Dagotto, Phys. Rev. B 73, 094434(2006).
- [11] H.J. Xiang, Su-Huai Wei, M.-H. Whangbo and Juarez L. F. Da Silva, Phys. Rev. Lett. **101**, 037209 (2008).
- [12] A. Malashevich and D. Vanderbilt, Phys. Rev. Lett. **101**, 037210 (2008).
- [13] X. Marti, V. Skumryev, C. Ferrater, M. V. Garc á-Cuenca, M. Varela, F. Sánchez,

- and J. Fontcuberta, Appl. Phys. Lett. 96, 222505 (2010).
- [14] T. Kimura, S. Ishihara, H. Shintani, T. Arima, K. T. Takahashi, K. Ishizaka, and Y. Tokura, Phys. Rev. B **68**, 060403 (2003).
- [15] T. Goto, T. Kimura, G. Lawes, A. P. Ramirez and Y. Tokura, Phys. Rev. Lett. **92**,257201 (2004).
- [16] C. J. Fennie and K. M. Rabe, Phys. Rev. Lett. **97**, 267602 (2006).
- [17] June Hyuk Lee, Lei Fang, Eftihia Vlahos, Xianglin Ke, Young Woo Jung, Lena Fitting Kourkoutis, Jong-Woo Kim, Philip J. Ryan, Tassilo Heeg, Martin Roeckerath, Veronica Goian, Margitta Bernhagen, Reinhard Uecker, P. Chris Hammel, Karin M. Rabe, Stanislav Kamba, Jürgen Schubert, John W. Freeland, David A. Muller, Craig J. Fennie, Peter Schiffer, Venkatraman Gopalan, Ezekiel Johnston-Halperin and Darrell G. Schlom, Nature **466**, 954 (2010).
- [18] See supplementary material for computational details, isosymmetric phase transition, and detailed study of electric polarization, Madelung energy calculation, Monte Carlo simulation result and double well structure.
- [19] B. G. Schlom, L.-Q. Chen, C.-B. Eom, K. M. Rabe, S. K. Streiffer and J.-M. Triscone, Annu. Rev. Mater. Res. 37, 589 (2007).
- [20] Y. R. Yang, W. Ren, M. Stengel, X. H. Yan and L. Bellaiche, Phys. Rev. Lett. **109**, 057602 (2012); A. T. Zayak, X. Huang, J. B. Neaton and K. M. Rabe, Phys. Rev. B **74**, 094104 (2006).
- [21] By mapping GGA+U calculations of the total energy for different collinear spin configurations onto Heisenberg Hamiltonian: $H = \sum_{i < j} \mathbf{S}_i \cdot \mathbf{S}_j$, our calculation leads to $J_{ab} = -1.93$ meV, $J_{aa} = 0.47$ meV, $J_{bb} = 0.70$ meV, and $J_{cc} = 0.62$ meV for bulk TbMnO₃ while $J_{ab} = -10.63$ meV, $J_{aa} = 2.53$ meV, $J_{bb} = 2.39$ meV, and $J_{cc} = -7.76$ meV for the epitaxially strained TbMnO₃.
- [22] A. J. Hatt, N. A. Spaldin and C. Ederer, Phys. Rev. B 81, 054109 (2010).
- [23] I. A. Sergienko, C. Sen and E. Dagotto, Phys. Rev. Lett. 97, 227204 (2006).
- [24] G. Giovannetti, S. Kumar, C. Ortix, M. Capone and J. van den Brink, Phys. Rev. Lett. **109**, 107601 (2012).
- [25] J. Samuel Smart and J. H. Van Vleck, Effective Field Theories of Magnetism

(Saunders Company, Philadelphia, 1966).

[26] S. Picozzi, K. Yamauchi, B. Sanyal, I. A. Sergienko and E. Dagotto, Phys. Rev. Lett. **99**, 227201 (2007).

[27] R. E. Cohen, Nature (London) 358, 136 (1992); C. Ederer and N. A. Spaldin, Phys. Rev. B 74, 024102 (2006).

FIGURES

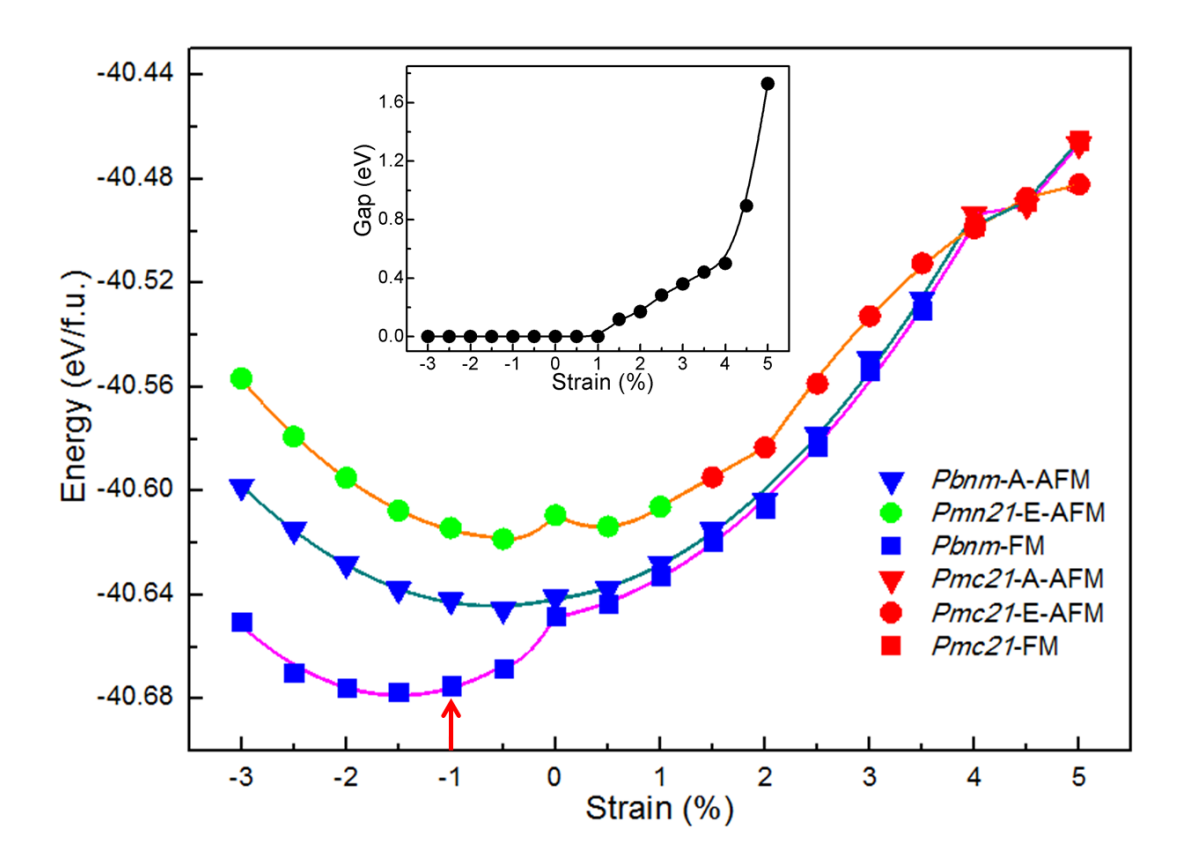


FIG. 1 (color online). Calculated total energy and band gap (insert) versus strain. Circle, down triangle and square represent E-AFM, A-AFM, FM spin orders, respectively. Red, green and blue colors label $Pmc2_1$, $Pmn2_1$ and Pbnm space group respectively. Red arrow hightlights the situation where (001)-oriented TbMnO₃ is epitaxially grown on the (001) plane of cubic substrate SrTiO₃.

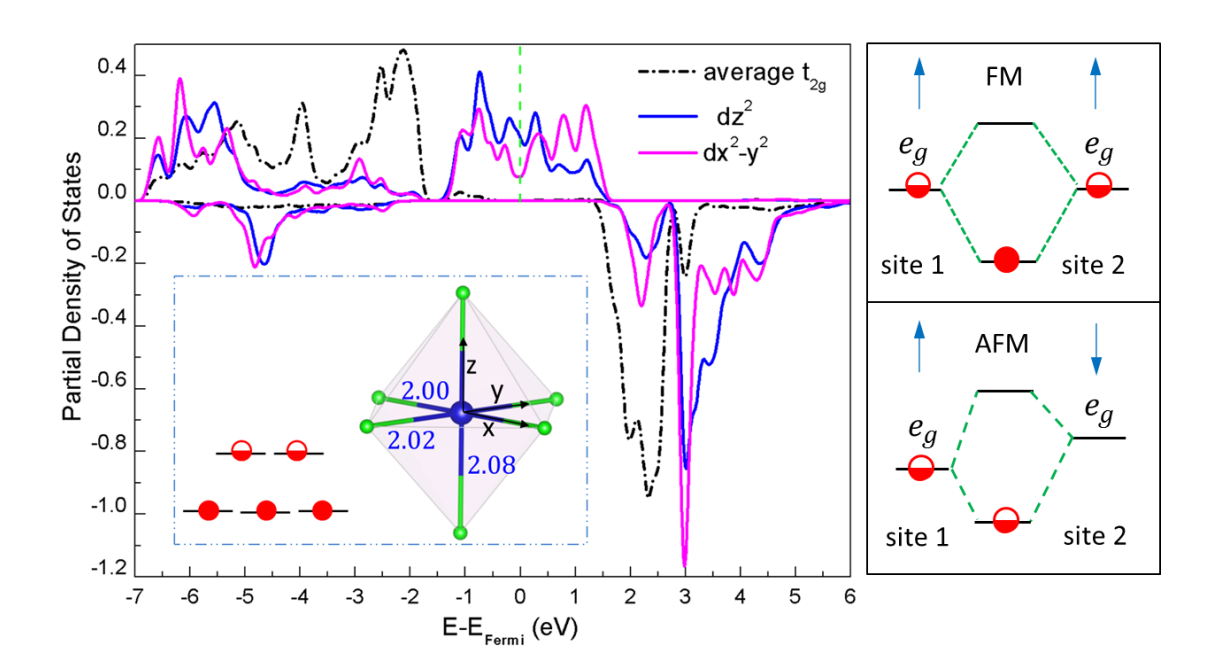


FIG. 2 (color on line). Left panel shows the Mn d-orbital partial density of state (PDOS). For simplicity, we plot the average t_{2g} PDOS. Insert are MnO₆ octahedron and electron configuration. Numbers give the Mn-O bond length in Å. Green vertical line gives Fermi energy level. Righ panel illustrates schematically the hybridization between e_g orbitals in FM (top) and AFM (bottom) cases. Half-filled circle represents half an electron. Spins are represented by arrows.

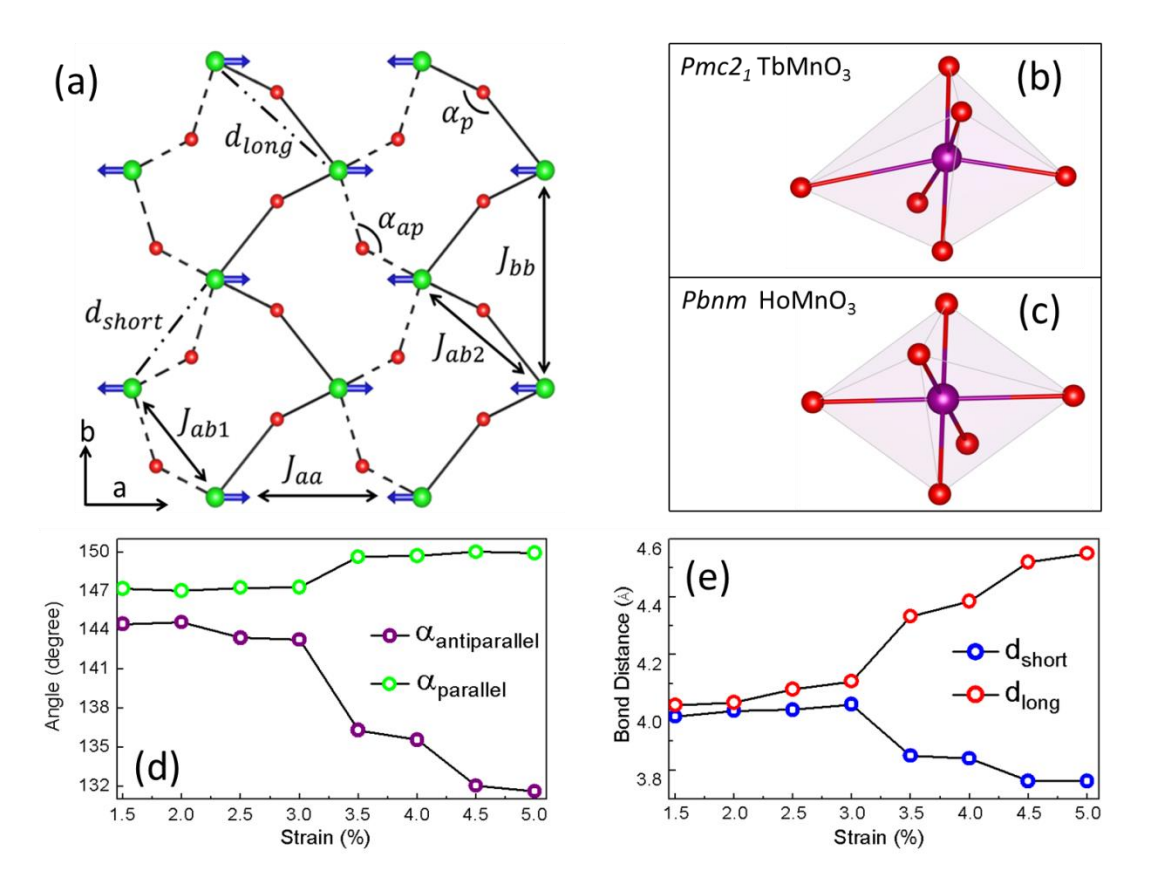


FIG. 3 (color online). (a) Illustration of E-type zigzag chains (solid lines). Large violet and small red spheres represent Mn and oxygen respectively. α_p , α_{ap} bond angles (see text), short (d_{short}) , long (d_{long}) Mn-Mn bonds, and exchange paths are denoted. MnO₆ octahedra of $Pmc2_1$ TbMnO₃ and bulk Pbnm HoMnO₃ are shown in (b) and (c), respectively. (d) Evolution of α_a , α_{ap} versus strain. (e) Evolution of d_{short} and d_{long} versus strain.

TABLE I. Total energy E_{tot} , elastic energy E_e and magnetic energy E_m for different states at 5% strain are listed.

strain	states	$E_{tot}(eV/f.u.)$	$E_e(eV/f.u.)$	$E_m(eV/f.u.)$
+5%	Pbnm-FM	-40.4412	-40.4243	-0.0169
+5%	Pmc2 ₁ -FM	-40.4706	-40.4688	-0.0019
+5%	Pmc2 ₁ -E-AFM	-40.4818	-40.4684	-0.0134

Supplementary Materials for

A New Multiferroic State with Large Electric Polarization in Tensile Strained $TbMnO_3 \label{eq:TbMnO3}$

Y. S. Hou, J. H. Yang, X. G. Gong*, and H. J. Xiang*

¹ Key Laboratory of Computational Physical Sciences (Ministry of Education), State Key Laboratory of Surface Physics, and Department of Physics, Fudan University, Shanghai 200433, P. R. China

1. Details of the density functional calculations

Our calculations were based on density functional theory (DFT) using generalized gradient approximation (GGA) plus the on-site Coulomb repulsion U method implemented in Vienna *ab initio* simulation package (VASP) [1-4]. In our calculation, an effective U value of 2 eV is applied to Mn *3d* states and a plane wave energy cutoff of 500 eV is used. Structural optimizations are performed toward equilibrium until the Hellmann-Feynman forces are less than 0.01 eV/Å. To calculate the electric polarization, we employ the Berry phase method [5].

2. Isosymmetric phase transition analysis

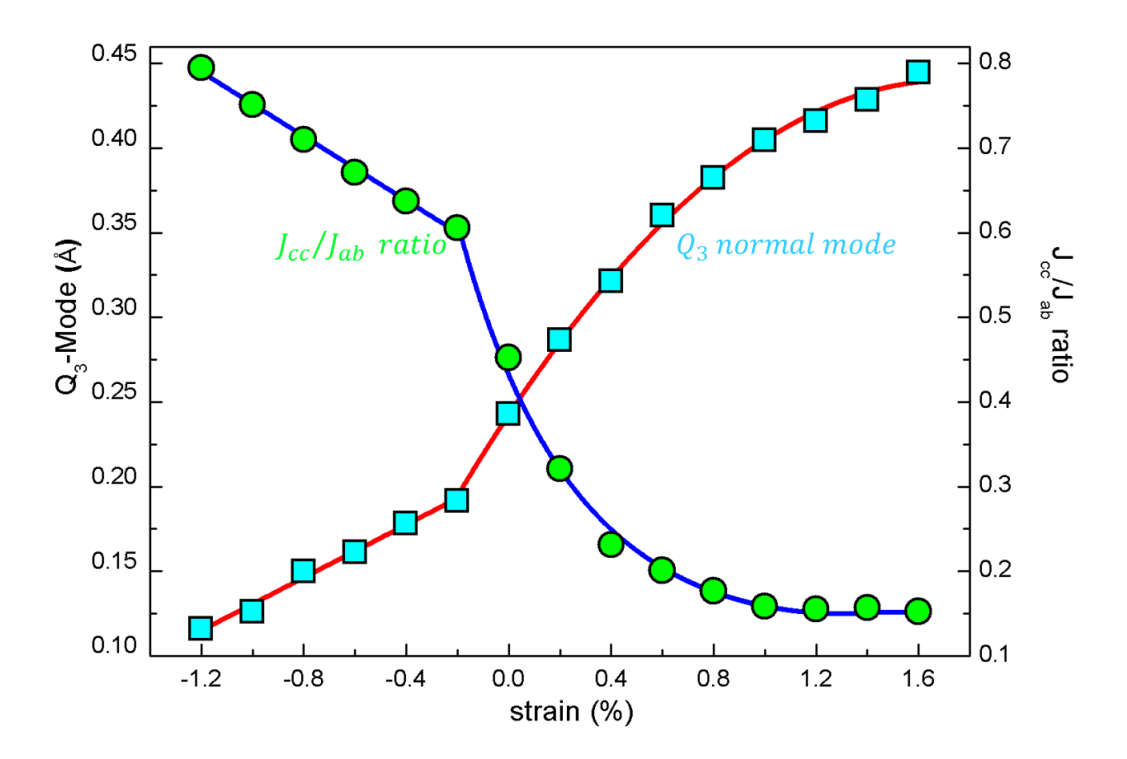


FIG. S1. Q_3 normal mode and J_{cc}/J_{ab} magnetic coupling ratio versus strain are shown, where J_{cc} is interlayer magnetic coupling and J_{ab} is intralayer nearest neighboring magnetic coupling.

It is clear that, Q₃ normal mode [6] characterizing the Jahn-Teller distortion of MnO₆ octahedron, and magnetic coupling ratio, sharply jump at the strain close to zero. Hence, there exists a discontinuous change in the internal coordinates of epitaxially strained TbMnO₃, i.e. a large structural reconstruction associated with a substantial change in the relative magnetic coupling strength. Detailed geometric structure analysis shows that the MnO₆ octahedron of epitaxially compressed TbMnO₃ is more regular than that of epitaxially tensile TbMnO₃ in terms of Mn-O bonds and O-Mn-O bond angles. This suggests that the isosymmetric phase transition is related to the internal structural change [7].

3. The electric polarization induced by the ion displacements

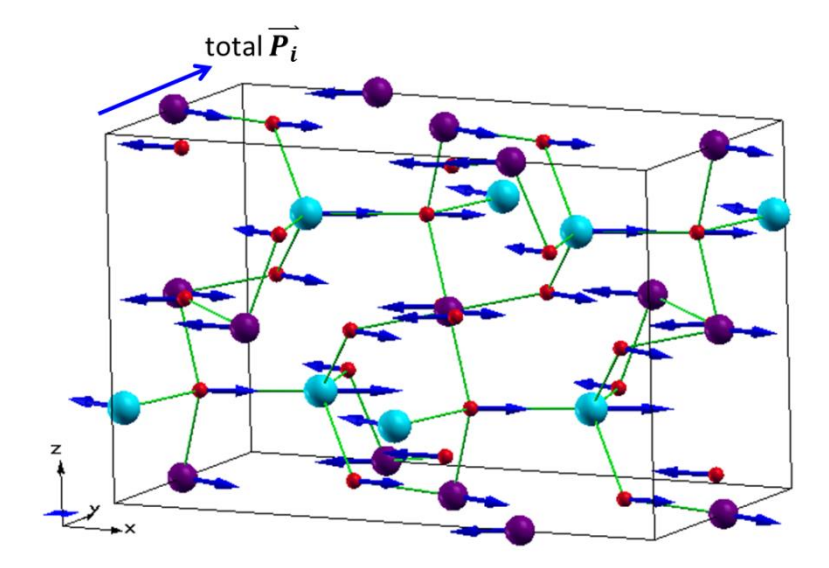


FIG. S2. Ion displacements and the total electric polarization \vec{P}_i are shown. Blue arrow presents the direction and magnitude of an ion's displacement. Violet, blue and red spheres are Manganite, Terbium and Oxygen, respectively.

The electric polarization induced by ion displacements from the centrosymmetric positions can be estimated through the Born effective charges (BEC) method [8]. The estimated electric polarization induced by the Terbium, Manganese and Oxygen ions are found to be $10.22~\mu\text{C}/cm^2$, $-1.90~\mu\text{C}/cm^2$ and $-4.41~\mu\text{C}/cm^2$, respectively. Hence the estimated electric polarization induced by ion displacements is $3.91~\mu\text{C}/cm^2$, along positive *b*-direction, consistent with our DFT calculated results. The inconsistency of polarization magnitude between these two methods is attributed to the substantial structure distortion and thereby the linear approximation of BEC method is not very accurate.

4. Investigation of Coulomb electrostatic interaction

In order to understand why ion displacements induce the above-mentioned electric polarization, Coulomb electrostatic interactions, i.e., Madelung energies, of some different structure configurations, whose lattice constants are fixed to that of $Pmc2_I$ -E-AFM structure in the case of 5% tensile strain, are calculated. Bader analysis indicates that Terbium, Manganese and Oxygen ions bear 2.21, 1.84 and -1.35 e respectively. Firstly, the centrosymmetric phase with Pbnm space group has a higher Madelung energy than that of $Pmc2_I$ -E-AFM structure by 0.14 eV/ion. In addition, given that all the internal coordinates of Terbium ions in the $Pmc2_I$ -E-AFM structure are replaced by that of centrosymmetric phase with Pbnm space group, denoting this structure as Tb-Pbnm- $Pmc2_I$, then the Tb-Pbnm- $Pmc2_I$ structure has a higher Madelung energy than $Pmc2_I$ -E-AFM structure by 0.07 eV/ion. Therefore, the ion displacements discussed above (and the electric polarization along positive b-direction) are favored by Coulomb electrostatic energy.

5. The electric polarization induced by the pure E-type magnetic order in HoMnO₃ and TbMnO₃, respectively

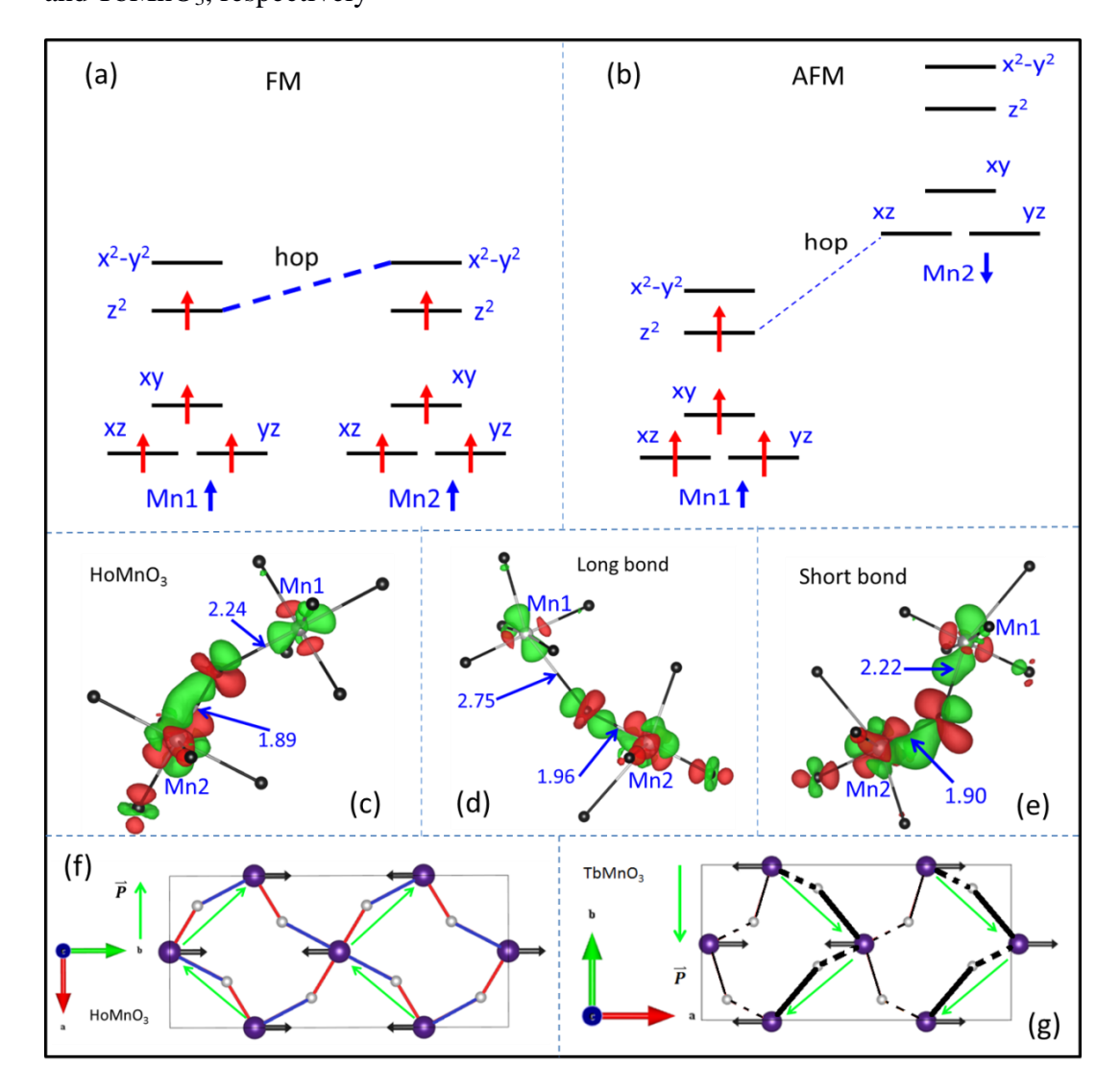


FIG. S3. Schematic illustration of the electron's hopping in the (a) FM case and (b) AFM case, respectively. Electron density difference $\Delta \rho = \rho(\uparrow,\uparrow) + \rho(\downarrow,\downarrow) - \rho(\downarrow,\uparrow) - \rho(\uparrow,\downarrow)$ for (c) bulk HoMnO₃, and (d) long Mn-Mn bond and (e) short Mn-Mn bond of the $Pmc2_1$ TbMnO₃ are plotted, where red color means $\Delta \rho > 0$ and the numbers give the Mn-O bond lengths in Å. Schematic illustrations of electric polarization induced by the pure E-type magnetic order are plotted for (f) bulk HoMnO₃ and (g) $Pmc2_1$ TbMnO₃, where green arrows depict the electric

polarization. In bulk HoMnO₃ (Fig. f), the red and blue lines stand for long and short Mn-O bonds, respectively. In *Pmc2*₁-E-AFM TbMnO₃ (Fig. g), solid lines and dashed lines stand for long and short Mn-O bonds, respectively.

First, let's investigate the d-electron hopping between two neighboring magnetic $\mathrm{Mn^{3+}}$ ions. In FM case, the e_g d-electron of Mn1 can hop to Mn2 (see Fig S3 a) because their d-orbital can strongly couple via the middle oxygen. However, in AFM case this hopping is negligible due to the very weak coupling since the coupled d-orbitals have a large energy difference (see Fig S3 b). This is also evidenced by the electron density difference plot shown in Figs S3 c, d and e. It is of importance to notice that, such hopping always leads to the homogenous migration of e_g electrons from the occupied d_{z^2} orbital of long Mn-O bond to the unoccupied $d_{x^2-y^2}$ orbital of short Mn-O bond. Based on this, pure E-type spin order produces an electric polarization along the negative a-direction in bulk HoMnO₃, consistent with the result of Ref 9, and along the negative b-direction in TbMnO₃ (see Figs S3 f and g), consistent with our DFT calculation results.

6. Monte Carlo simulation for the transition temperature in the case of 5% epitaxially strained $TbMnO_3$

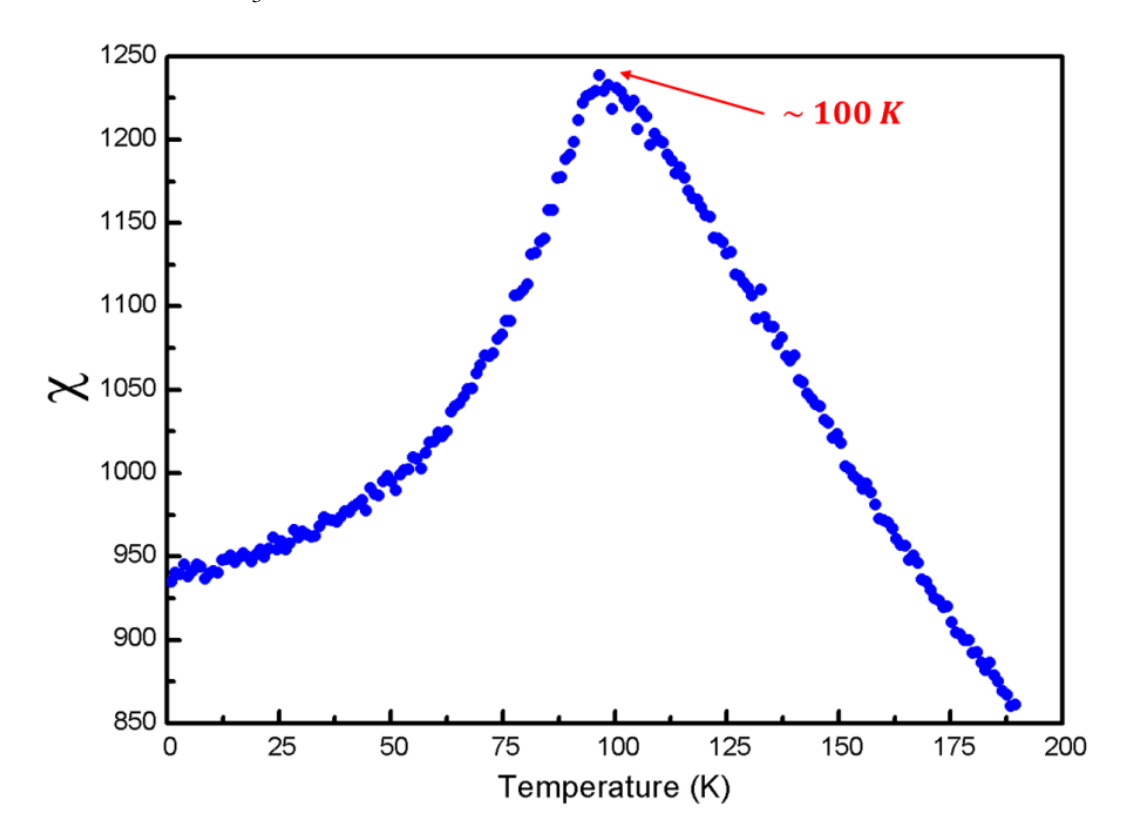


FIG. S5. Magnetic susceptibility as a function of temperature from the Monte Carlo simulation. Clearly, a peak appears at about 100~K, indicating a phase transition from the paramagnetic state to the E-AFM state. It is well-known that the classical Monte Carlo underestimates the transition temperature. Thus, we expect that the transition temperature of the $Pmc2_1$ -E-AFM state is above 100 K.

7. Double well structure for $Pmc2_1$ -E-AFM state in the case of 5% epitaxially strained TbMnO₃

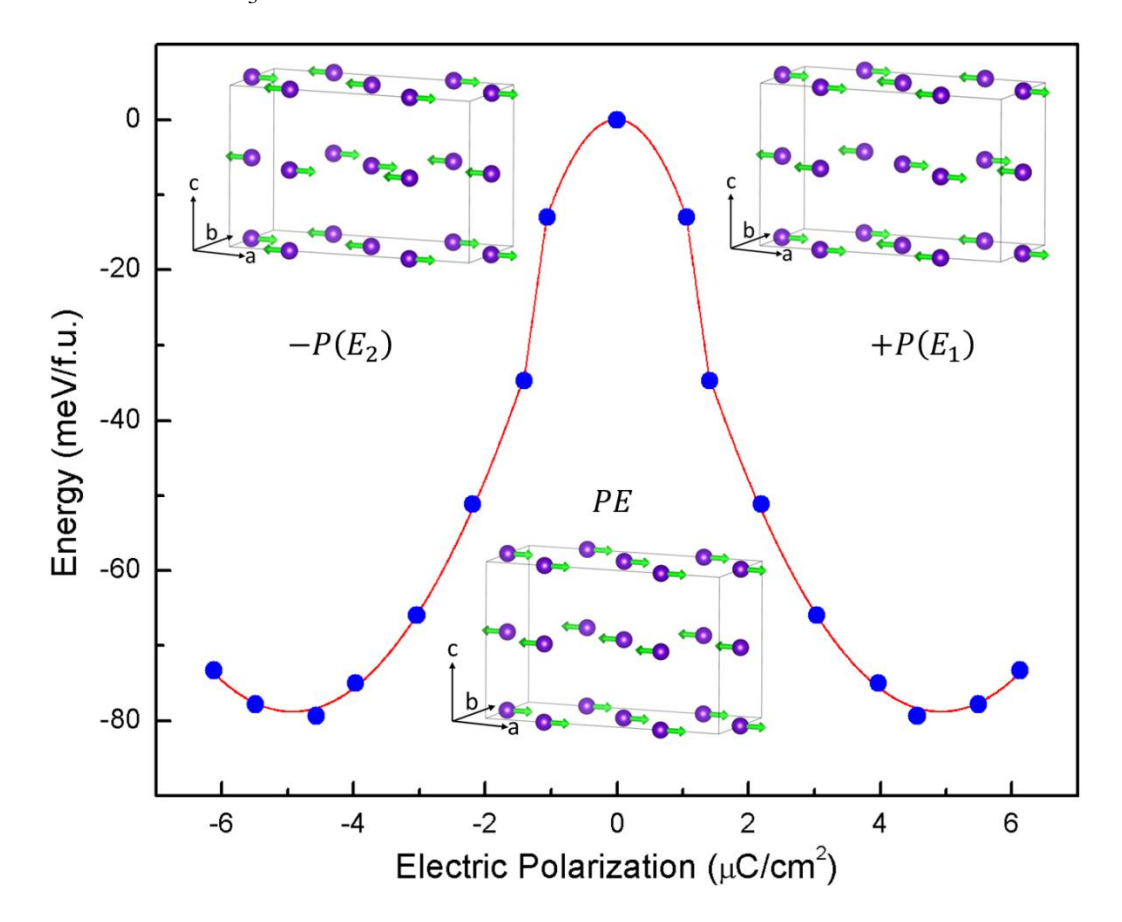


FIG. S6 (color online). Calculated electric polarization (μ C/cm²) versus energy (meV/formula unit). Inserts are antiferromagnetic domains -P(E2), +P(E1) and antiferromagnetic paraelectric phase respectively. Only Mn³⁺ ions are shown.

Reference

- [1] A. I. Liechtenstein, V. I. Anisimov and J. Zaanen, Phys. Rev. B 52, R5467 (1995).
- [2] J. P. Perdew, K. Burke and M. Ernzerhot, Phys. Rev. Lett. 77, 3865 (1996).
- [3] P. E. Blochl, Phys. Rev. B 50, 17953 (1994); G. Kresse and D. Joubert, Phys. Rev. B 59, 1758 (1999).
- [4] G. Kresse and J. Furthmuller, Phys. Rev. B **54**, 11169 (1996).
- [5] R. D. King-Smith and D. Vanderbilt, Phys. Rev. B 47, 1651 (1993); R. Resta, Rev. Mod. Phys. 66, 899 (1994).
- [6] E. Dagotto, T. Hotta and A. Moreo, Physics Reports 344, 1 (2001).
- [7] A. G. Christy, Acta Cryst. B **51**, 753 (1995).
- [8] J. B. Neaton, C. Ederer, U. V. Waghmare, N. A. Spaldin, and K. M. Rabe, Phys. Rev. B 71, 014113 (2005)
- [9] I. A. Sergienko, C. Sen and E. Dagotto, Phys. Rev. Lett. 97, 227204 (2006).